INFLUENCE OF TURBULENCE ON THE STABILITY OF LIQUID SHEETS

K. Heukelbach, S. Jakirlić, R. Nakić*and C. Tropea
Kai.Heukelbach@sla.tu-darmstadt.de
FG Strömungslehre und Aerodynamik
Technische Universität Darmstadt
Petersenstr. 30, 64287 Darmstadt / Germany

Abstract
In this work the influence of turbulence on the stability of liquid films was studied. A nozzle was used that produced different turbulent levels, while the Reynolds and Weber numbers were kept the same. In former work (Heukelbach and Tropea, 2001 [2]) it was stated that turbulence stabilizes the liquid film by decreasing the growth of capillary waves. However, at certain turbulence levels it was found that ligaments detached from the liquid surface directly, without apparent wave growth. With the help of numerical calculations this behavior was related to an increase of the turbulent stresses normal to the liquid surface.

Introduction
In many applications the prediction of atomization or disintegration of liquid sheets and jets is intimately related to understanding the stability problem under various operating conditions. One influencing parameter is the level of turbulent flow fluctuations at the nozzle exit, since this represents the perturbations entering any stability analysis [10], [5]. However, turbulence acts in different ways on the stability of films and jets. On the one hand, it increases the initial disturbance level, which promotes instability according to a linear analysis [8]. On the other hand, it reduces the growth of capillary waves and leads to increased stability for liquid films, which was shown by [2]. For high enough turbulence levels however, a direct disruption of ligaments from the liquid surface can be observed. It is believed that these deformations are caused by an increase of turbulent stresses normal to the liquid surface. This statement has not yet been verified by experiments, since the velocity measurements by [2] only provided turbulence quantities in the mean flow direction.

In the present work, a special nozzle was used that produces different levels of turbulence, while the characteristic Reynolds and Weber numbers were held constant. So the differences in the liquid film instability can be related to the changes in the turbulence structure only. In order to achieve a better understanding of the turbulence situation inside the nozzle, numerical calculations are performed, focused especially on the behavior of the turbulent normal stresses. For special cases, the numerical results are verified by the LDV measurements performed in [2].

Experimental setup
The experimental setup is identical with that of [2] and the nozzle is a further development of nozzle B. It consists of a plane channel of $650\mu m$ height and $22mm$ depth. In the upstream direction cavities are cut into the channel walls. At the bottom of these cavities, four small holes are drilled into the wall. Bypass tubes connect these holes with the main liquid supply. The nozzle can be operated in two modes. In the first mode, the bypass tubes are closed and the total flux is supplied through the main channel of the nozzle. In this condition the nozzle represents exactly the case of nozzle B in [2]. In the second mode, the main liquid supply is split into the main flow and a bypass flow, which is guided through the tubes and eventually enters the nozzle through the cavities. A sketch of the nozzle geometry is given in Fig. 1.

The total volume flux and the static pressure in the upstream channel, before the contraction of the nozzle, can be measured. The partial volume flux through the cavities is estimated using a momentum

*On leave from the University of Sarajevo, Bosnia Herzegovina

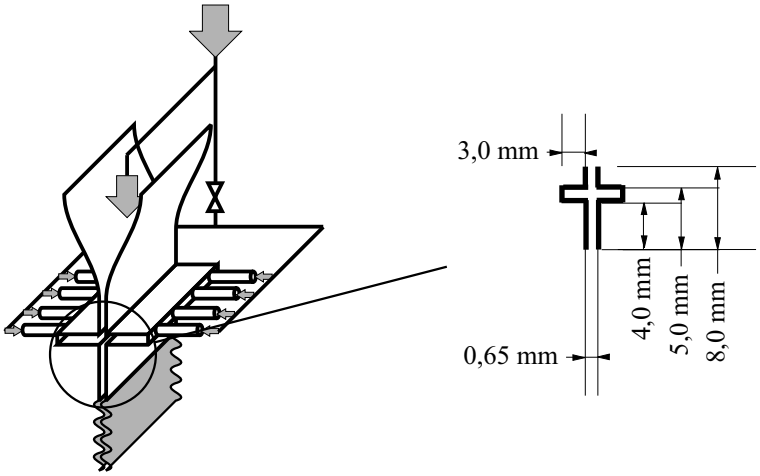

Fig. 1: Sketch of nozzle and bypass flow into nozzle sidewalls

balance and neglecting sidewall forces in the cavities. With this approximation, the volume flux through the cavities was approximately 5% of the total flux when the tubes were opened.

The Re and We number for characterization of the liquid film are computed using quantities at the nozzle exit. Thus, for both modes the characteristic parameters describing instability phenomena are constant, while the turbulence quantities of the flow are changed. The liquid film instability will be studied by back-lit photography. The corresponding flow conditions within the nozzle will be described with the help of numerical calculations.

Computational method

All computations were performed by a computer code based on a finite-volume numerical method for solving the Reynolds Averaged Navier-Stokes equations in orthogonal coordinate systems with a collocated variable arrangement. The primary variables are the cartesian velocity and Reynolds stress tensor components and pressure. The velocity-pressure coupling is ensured by the pressure correction method based on the well-known SIMPLE algorithm. The equations are linearized and solved sequentially using an iterative ILU method. A special, selective interpolation procedure, involving the interpolation of equations, i.e. its terms, instead of the variables themselves, was applied for velocity-stress coupling. Diffusion fluxes are approximated by central differences (CD). For discretization of the convective fluxes, a blended upwind-central differencing scheme, implemented in the so-called deferred-correction manner was used for the computations with low-Reynolds number models. For the computations with high-Reynolds number models a second-order, linear upwind differencing scheme (LUDS) was applied.

The dimensions and shape of the solution domain used are shown in Fig. 7. The numerical grid used for high and low-Reynolds number model computations employed 200x100 and 300x150 control volumes respectively. The grid was squeezed in the near-wall regions, providing the dimensionless wall distance y^+ of the numerical node closest to the wall being $\approx 10-15$, when using high-Reynolds models in conjunction with the so-called wall functions, i.e. ≤ 0.5, if low-Re models were applied. Standard wall functions were used for high-Reynolds number model computations.

Computations were performed with two two-equation models: the standard $k-\varepsilon$ high-Re model and with its low-Re extension due to Jones and Launder (1972), as well as with two types of the Reynolds-stress turbulence models: the model of Speziale, Sarkar and Gatski - SSG (1991) with quadratic formulation of the pressure scrambling process, Φ_{ij}, and with the low-Re number version of the second-moment (Reynolds stress) closure model, denoted as HJ low-Re SMC (Hanjalic and Jakirlic, 1998). The latter model contains the modifications for viscosity and wall blockage effects, being modelled in terms of invariant local turbulence parameters, such as invariants of the anisotropy of Reynolds-stress and dissipation-rate tensors, as well as turbulence Reynolds number (see [1] for further details). The $k-\varepsilon$ models served mainly for the initialization of the mean flow and turbulence fields. In addition to the non-linear formulation of both the slow ($\Phi_{ij,1}$) and rapid ($\Phi_{ij,2}$) parts of the pressure strain term, the SSG model was further modified to account for the anisotropies in the dissipation process (ε_{ij}) by applying the non-linear model of Hallbäck et al. (see [7] for more details). The pressure redistribution and dissipation terms can be now

presented jointly:

$$\Phi_{ij,1} + \Phi_{ij,2} - \varepsilon_{ij} = -C_1 \varepsilon a_{ij} - (C_1' + \alpha)\varepsilon \left(a_{ik}a_{kj} - \frac{1}{3}A_2\delta_{ij} \right) - C_2' a_{ij} P_k + C_3 k S_{ij}$$
$$+ C_4 k \left(a_{ip}S_{pj} + a_{jp}S_{pi} - \frac{2}{3}a_{pq}S_{pq}\delta_{ij} \right) + C_5 k \left(a_{ip}\Omega_{pj} + a_{jp}\Omega_{pi} \right) - \left[(1 - f_s)\frac{2}{3}\delta_{ij}\varepsilon + f_s \frac{\overline{u_i u_j}}{k}\varepsilon^h \right]$$

where $\alpha = 3/4$ and $f_s = 1 + \alpha(A_2/2 - 2/3)$ (see [11] for other model coefficients).

Results and discussion

In this section some exemplary cases of parameter setups will be described. All experiments are performed with water. The results are shown in Fig. 2–5. On the left side, the operating mode for closed tubes is shown, whereas on the right side the tubes are open: the global parameters remain the same.

In Fig. 2 on the left side one can see the classical behavior of liquid film instability. The liquid exits

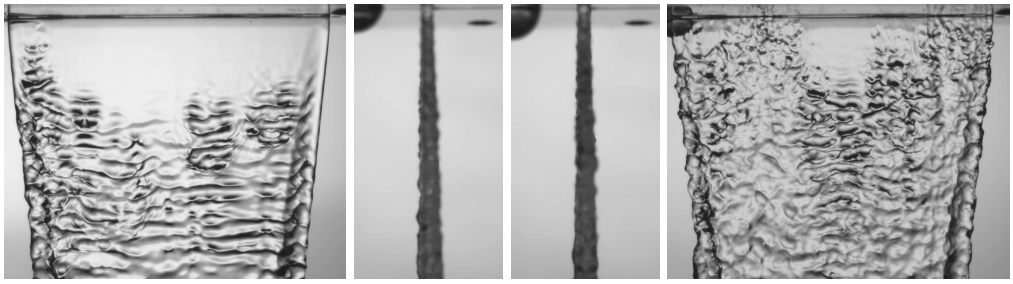

Fig. 2: $Re \approx 3000; We \approx 200$ (left: closed tubes; right: open tubes)

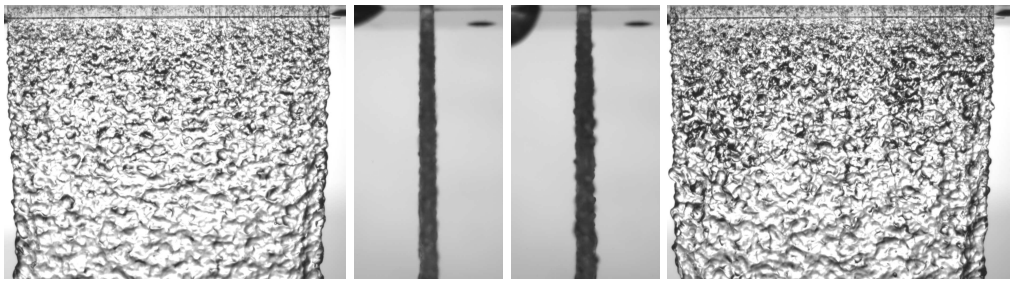

Fig. 3: $Re \approx 6000; We \approx 700$ (left: closed tubes; right: open tubes)

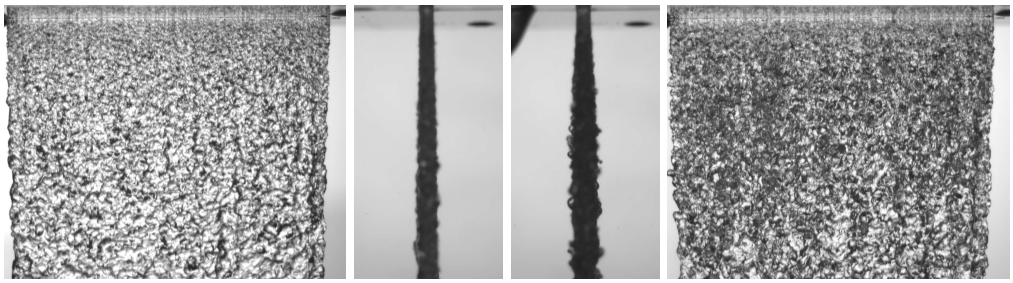

Fig. 4: $Re \approx 10000; We \approx 2300$ (left: closed tubes; right: open tubes)

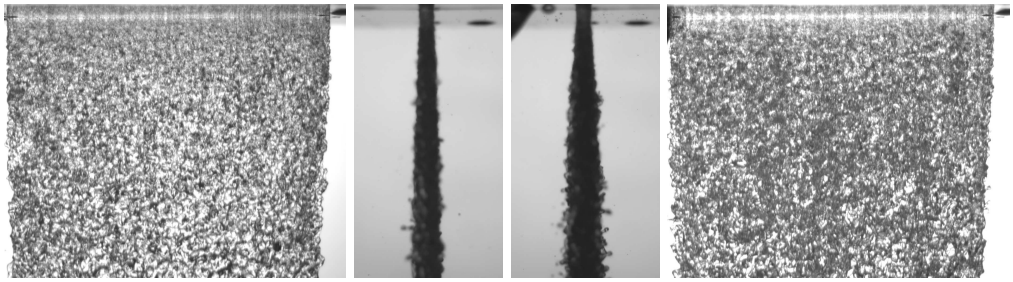

Fig. 5: $Re \approx 14000; We \approx 4000$ (left: closed tubes; right: open tubes)

the nozzle, forming a rather smooth surface. In the downstream direction small capillary waves can be observed, that slowly grow in amplitude. This behavior is well known from linear instability analysis and it was demonstrated in [2] that the flow inside the nozzle must be more or less laminar in order to make this phenomena visible. On the other hand, for the case of medium turbulence intensities, the growth of capillary waves is suppressed and the film remains intact, which was shown in [3]. However, for turbulent flows an immediate roughening of the free liquid surface can be observed after exiting the nozzle. In downstream direction, this roughness smoothes due to surface tension forces. On the right side of Fig. 2 an intermediate stage of the above described cases can be observed. There is still a partial existence of capillary waves, but due to disturbances induced by the volume flux coming from the cavities, a certain additional waviness occurs on the surface.

In Fig. 3 the turbulence in the flow, induced by the cavities, is already high enough in both modes to suppress the growth of capillary waves. However, on the right side it can be seen, that the elevation of the random surface disturbances is bigger than for the case of closed tubes (side view). This behavior becomes even more evident when the exit velocity is increased as in Fig. 4. For high enough disturbance levels, the ligaments detach from the surface, which can be observed in Fig. 5. This case can be referred to as direct atomization, which is mainly used in the context with round liquid jets.

However, for all cases it can be stated that the spread of the liquid surface is always stronger for the mode of opened tubes. Since for this situation a part of the flux enters the main nozzle flow perpendicularly, the turbulence level is expected to be higher in the channel than without the tubes open. It is believed from [2], that the observed roughening of the exit jet surface is mainly caused by turbulent stresses normal to the liquid surface. However, there is no quantitative measure to prove this statement yet. Therefore numerical simulations have been performed to focus especially on the effect of altering turbulent stress levels.

Selected numerical results of all three configurations investigated: flat nozzle (denoted throughout the article as nozzle A, see [2]) and nozzle B with closed and open tubes are compared with available experimental results in Figs. 6-8. Before starting with the computations of the nozzles B, representing a flow

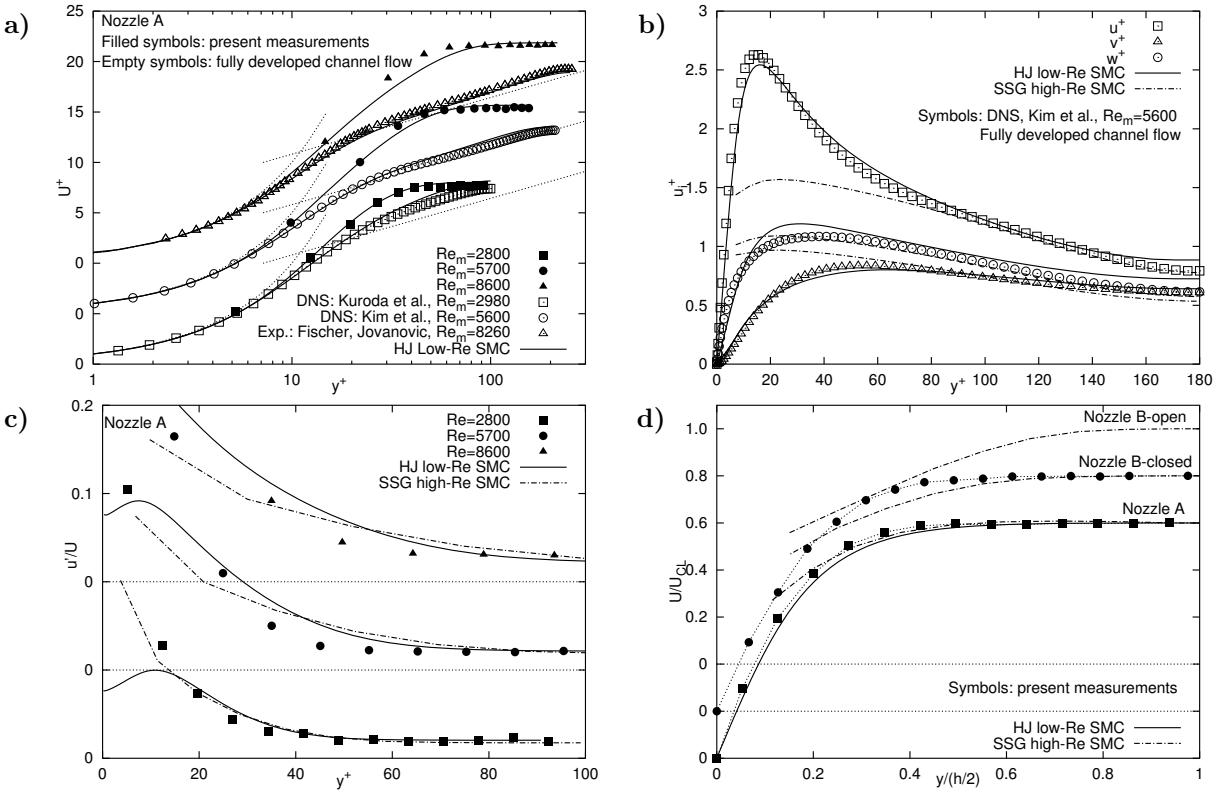

Fig. 6: a), b) and c) Turbulence model validation: semi-log plots of the mean velocities and turbulent stress components for a developing (nozzle A) and fully developed channel flow and d) mean velocity profiles at a selected cross-section for all three nozzle configurations computed

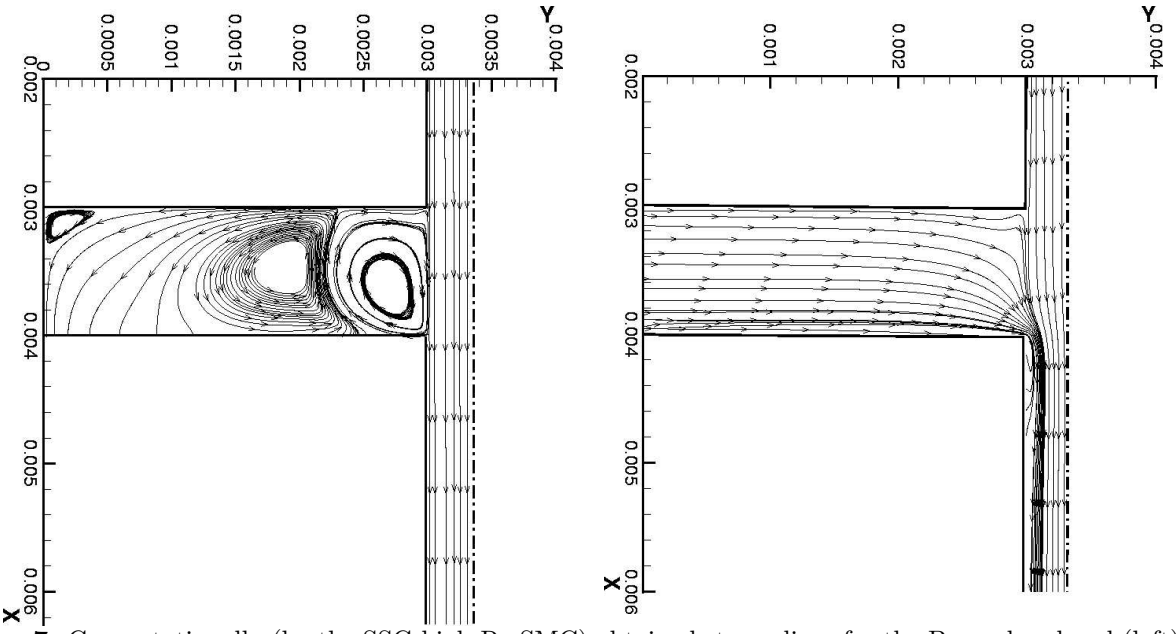

Fig. 7: Computationally (by the SSG high-Re SMC) obtained streamlines for the B nozzle: closed (left) and open (right)

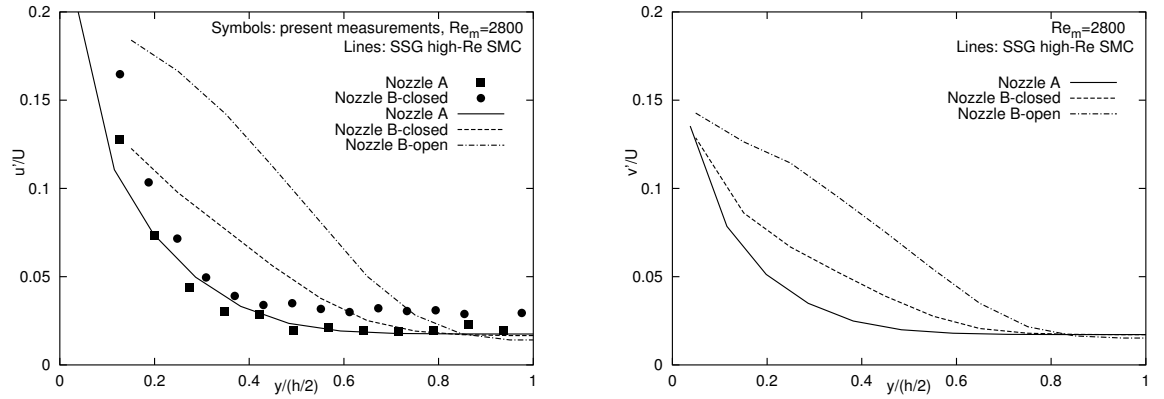

Fig. 8: Streamwise and normal-to-the-wall turbulence intensities at a selected cross-section for all three nozzle configurations computed

over a closed and open cavity, the developing (as in the case of the nozzle A) and fully developed channel flows were computed in order to validate the turbulence models used. In addition to the results of the present measurements, some other relevant experimental data as well as the results of direct numerical simulations of channel flows with almost identical bulk Reynolds numbers were taken for comparison. Fig. 6a shows the semi-log plots of the mean velocity profiles for both channel flows (developing and fully developed) for all three Reynolds numbers investigated. The differences in the mean flow structure are clearly represented. The velocity profiles across the developing flow (nozzle A) point out a certain deviation from the logarithmic law, illustrating a superiority of the low-Reynolds number models (see also Fig. 6b), whose near-wall modifications allow the integration of the model equations up to the wall itself. Despite of this fact, the high-Re models, using the wall functions for the bridging the viscosity affected near-wall region, could be successfully applied in the logarithmic law region and outer layer ($y^+ \geq 40$) even at such a low Reynolds number range. Fig. 6c displays the streamwise turbulence intensities for the nozzle A. The thickening of the wall proximity affected region expressed in the wall coordinates (y^+) by Reynolds number increasing is obvious. The qualitative and quantitative agreement with both model groups is reasonable. The computationally obtained streamlines for the nozzles B are depicted in Figs. 7. The secondary flow in a cavity with the closed tubes seems to be very intensive. However, the velocity vector plots (not shown here) reveal that this impression is wrong. The velocity amplitudes in this flow region are very small. It seems that the vortical structures created in the cavity decelerate to some extent

the mean flow in the nozzle (see comparison of the linear plots of the mean velocity profiles in Fig. 6d) leading to an increasing in both the streamwise and normal-to-the-wall turbulence intensities, Fig. 8. This flow deceleration (clearly visible in Fig. 6d) is much more intensive in the case with the open tubes. By opening the tubes an additional flow rate streams into the cavity (Fig. 7 right), generating a separation bubble immediately after both streams are unified in the nozzle. The bubble creation intensified mean shear, which is the main source of the turbulence production. This is confirmed in Figs. 8, showing significant increase in turbulence intensity. This fulfills the statements coming out from the experimental investigations, that the increased turbulence intensity (especially its normal component) in the nozzle is closely related to the roughening of the liquid sheet surface. The low-Reynolds model computations of the nozzles B are in progress.

Conclusions

The main objective of this work was to investigate how turbulence influences the stability of liquid films. Based on the work of [2] it can be stated, that turbulence reduces the growth of capillary waves and therefore stabilizes the liquid film. If on the other hand turbulence is increased to a certain level, it can cause the liquid to form ligaments directly separated from the surface without subsequently wave growth. Bearing in mind the results of the shown nozzle in the two operating modes, this effect may be related to an increase in the turbulent stress normal to the liquid surface, namely $-\varrho\,\overline{v'^2}$. This statement is supported by the numerical calculations, that show a systematic increase of the v' component when the bypass tubes are open. However, the results still lack of a quantitative relation between the increased turbulence level and the elevation of the surface disturbances. This measure would be easier to realize for round liquid jets, since they provide better optical access to the observed phenomena.

References

[1] **K. Hanjalic, S. Jakirlic**, "Contribution Towards the Second-Moment Closure Modelling of Separating Turbulent Flows", *Computers and Fluids*, Vol. 22, No. 2, pp 137-156, 1998

[2] **K. Heukelbach, C. Tropea**, "Influence of the inner flowfield of flat fan pressure atomizers on the disintegration of the liquid sheet", *17th Annual Conference on Liquid Atomization and Spray Systems*, ILASS Europe, Zurich, 2001

[3] **K. Heukelbach, C. Tropea**, "Einfluss der Düseninnenströmung auf den Zerfallsmechanismus bei Flachstrahldruckzerstäubern", *Spray 2001*, Hamburg, 2001

[4] **H. Hiroyasu, M. Arai, M. Shimizu**, "Effect of Flow Conditions Inside Injector Nozzles on Jet Breakup Processes", *Recent Advances in Spray Combustion: Spray Atomization and Drop Burning Phenomena Volume 1*, American Institute of Aeronautics and Astronautics Inc., vol 166, pp. 173-184, 1996

[5] **I. Kim, W. A. Sirignano**, "Three-dimensional wave distortion and disintegration of thin planar liquid sheets", *J. Fluid Mech.*, vol. 410, pp. 147-183, 2000

[6] **W.P. Jones, B.E. Launder** "Some Properties of Sink-Flow Turbulent Boundary Layers", *J. Fluid Mech.*, Vol. 56, part 2, pp 337-351, 1972

[7] **J. Knöll, S. Jakirlić, K. Hanjalić**, "A priori Assessment of Algebraic and Differential Reynolds-Stress Models using DNS Database", *2nd International Symposium on Turbulent Shear Flows Phenomena*, June 27-29, Stockholm, Sweden

[8] **X. Li**, "Spatial instability of plane liquid sheets", *Chemical Engineering Science*, vol. 48, n. 16, pp. 2973-2981, 1993

[9] **A. Mansour, N. Chigier**, "Effect of Turbulence on the Stability of Liquid Jets and the Resulting Droplet Size Distributions", *Atomization and Sprays*, vol. 4, pp. 583-604, 1994

[10] **C. Mehring, W. A. Sirignano**, "Nonlinear capillary wave distortion and disintegration of thin planar liquid sheets", *J. Fluid Mech.*, vol. 388, pp. 69-113, 1999

[11] **C.G. Speziale, S. Sarkar, T.B. Gatski**, "Modelling the Pressure-Strain Correlation of Turbulence: an Invariant Dynamical Systems Approach", *J. Fluid Mech.*, Vol. 227, pp. 245-272, 1991

[12] **N. Tamaki, K. Nishida, H. Hiroyasu**, "Promotion of the atomization of a liquid jet by cavitation in a nozzle hole", ILASS-Europe, Manchester 1998, pp.218-223

[13] **P.-K. Wu, R. F. Miranda, G. M. Faeth**, "Effects of Initial Flow Conditions on Primary Breakup of Nonturbulent and Turbulent Round Liquid Jets", *Atomization and Sprays*, vol. 5, pp. 175-196, 1995